Journal of Biomechanics 83 (2019) 134–142

Contents lists available at ScienceDirect

Journal of Biomechanics

journal homepage: www.elsevier.com/locate/jbiomech
www.JBiomech.com

A calibrated EMG-informed neuromusculoskeletal model can appropriately account for muscle co-contraction in the estimation of hip joint contact forces in people with hip osteoarthritis

Hoa X. Hoang, Laura E. Diamond *, David G. Lloyd, Claudio Pizzolato

School of Allied Health Sciences, Griffith University, Gold Coast 4222, Australia
GCORE, Menzies Health Institute Queensland, Griffith University, Gold Coast 4222, Australia

ARTICLE INFO

Article history:
Accepted 23 November 2018

Keywords:
EMG-assisted
Static optimisation
CEINMS
OpenSim
Hip
Osteoarthritis
Neural control solution

ABSTRACT

Abnormal hip joint contact forces (HJCF) are considered a primary mechanical contributor to the progression of hip osteoarthritis (OA). Compared to healthy controls, people with hip OA often present with altered muscle activation patterns and greater muscle co-contraction, both of which can influence HJCF. Neuromusculoskeletal (NMS) modelling is non-invasive approach to estimating HJCF, whereby different neural control solutions can be used to estimate muscle forces. Static optimisation, available within the popular NMS modelling software OpenSim, is a commonly used neural control solution, but *may not* account for an individual's unique muscle activation patterns and/or co-contraction that are often evident in pathological population. Alternatively, electromyography (EMG)-assisted neural control solutions, available within CEINMS software, have been shown to account for individual activation patterns in healthy people. Nonetheless, their application in people with hip OA, with conceivably greater levels of co-contraction, is yet to be explored. The aim of this study was to compare HJCF estimations using static optimisation (in OpenSim) and EMG-assisted (in CEINMS) neural control solutions during walking in people with hip OA. EMG-assisted neural control solution was more consistent with both EMG and joint moment data than static optimisation, and also predicted significantly higher HJCF peaks ($p < 0.001$). The EMG-assisted neural control solution also accounted for more muscle co-contraction than static optimisation ($p = 0.03$), which probably contributed to these higher HJCF peaks. Findings suggest that the EMG-assisted neural control solution may estimate more physiologically plausible HJCF than static optimisation in a population with high levels of co-contraction, such as hip OA.

1. Introduction

Hip osteoarthritis (OA) is a degenerative and debilitating disease that poses a significant burden on the healthcare system (Wang et al., 2011). OA has no cure, and conservative treatments to reduce pain and improve function remain only modestly effective (Murphy et al., 2016). The progression of hip OA can be rapid, with almost 40% of people with symptomatic hip OA undergoing a total hip replacement (THR) within 2-years following diagnosis (Gossec et al., 2005). THR is a last resort as it is costly and invasive; hence, conservative treatments must improve to slow disease progression and maintain quality of life for OA sufferers. Abnormal hip joint contact forces (HJCF) are considered a primary mechanical risk factor for the initiation and progression of hip OA (Felson, 2013). An understanding of HJCF in the native joint is therefore critical to provide new insight into the pathology and to advance conservative treatments for people with hip OA. Instrumented hip implants have been used to measure *in-vivo* HJCF (Bergmann et al., 2016; Brand et al., 1994); however, estimating *in-vivo* HJCF in people with hip OA remains a challenge, as direct measurement is invasive and may not represent loading in the native joint.

Computational neuromusculoskeletal (NMS) modelling is a non-invasive alternative to estimate contact forces in the native joints during dynamic movements (Arnold and Delp, 2005; van den Bogert et al., 1999). NMS models parameters can be calibrated to an individual, then different algorithms or neural solutions can be used to estimate muscle activation patterns, and subsequently muscle-tendon forces and joint contact forces (JCF). The freely available modelling software OpenSim (Delp et al., 2007) implements a static optimisation (SO) neural solution that minimises

* Corresponding author at: GCORE, Menzies Health Institute Queensland, GriffithUniversity, Gold Coast 4222, Australia.
E-mail address: l.diamond@griffith.edu.au (L.E. Diamond).

https://doi.org/10.1016/j.jbiomech.2018.11.042
0021-9290/

muscle activations and has been regularly used to estimate JCF at the hip (Giarmatzis et al., 2015; Graham et al., 2016; Skalshøi et al., 2015; Wesseling et al., 2016b). However, musculoskeletal parameters are usually not calibrated when using SO and limitations exist when investigating the hip joint, such as differences between SO results and EMG recorded from hip muscles (Anderson and Pandy, 2001) or inability to predict co-contraction observed in individuals with hip OA (Park et al., 1999; Zeni et al., 2010). Thus, SO may not well predict hip muscle activation patterns, muscle co-contractions, and consequently, hip muscle forces and HJCF in this patient population (Anderson and Pandy, 2001; Challis, 1997; Gottlieb, 2000; Hughes et al., 1995).

OpenSim can also employ several EMG-informed neural solutions that are calibrated to the individual to improve JCF estimates (Gerus et al., 2013; Hoang et al., 2018) and use a combination of optimisation and experimental EMG signals to solve for the activation patterns (Gerus et al., 2013; Konrath et al., 2017; Lloyd and Besier, 2003; Lloyd and Buchanan, 1996; Manal and Buchanan, 2013; Pizzolato et al., 2015; Saxby et al., 2016a, 2016b; Thelen et al., 1994; Wellsandt et al., 2016), and have been used to estimate HJCF (Hoang et al., 2018). Specifically, the EMG-assisted method is an EMG-informed neural solution mode which: (i) synthesises excitations for muscles that are difficult to record, (ii) adjusts experimental muscle excitations to mitigate the errors associated with surface EMG (e.g. crosstalk, poor electrode placement, skin impedance) (Farina and Negro, 2012), and (iii) improves joint moment tracking. Although the EMG-assisted method is a promising alternative to SO in estimating HJCF, it has never been used to estimate HJCF to investigate individuals with hip OA, nor evaluated against direct measures from instrumented hip implants (Bergmann et al., 2016).

This study aimed to: (1) determine whether EMG-assisted method (Pizzolato et al., 2015; Sartori et al., 2014) can estimate physiologically plausible HJCF in people with hip OA; (2) determine if the EMG-assisted method can better account for muscle co-contraction compared to SO; and (3) compare HJCF estimates from EMG-assisted and SO methods with instrumented hip implant data (Bergmann et al., 2016). We hypothesised that the EMG-assisted method will: (1) estimate more physiologically plausible HJCF in individuals with hip OA, (2) better account for muscle co-contraction, and (3) generate HJCF estimates closer to instrumented data compared to SO.

2. Methods

This study's research ethics was approved by Griffith University's Human Research Ethics Committee and all participants gave their written informed consent before participation. The study's 18 participants (age = 64.0 ± 7.0 yr, body mass = 76.8 ± 14.1 kg, height = 166.0 ± 9.1 cm) had radiographic hip OA (Kellgren-Lawrence grade 2 or 3 (Kellgren and Lawrence, 1957)) with Harris Hip Scores $\leq$ 95 (Mahomed et al., 2001). Nine participants were diagnosed with bilateral symptomatic and radiographic hip OA, with the study limb being the more affected side. Participants were excluded if they had other major lower limb musculoskeletal or neurological conditions.

A full-body set of retro-reflective markers (Graham et al., 2014) was affixed to the participants. A 12-camera motion analysis system (Vicon, Oxford, UK) recorded marker trajectories (200 Hz); two force plates (Kistler, Amherst, USA) recorded ground reaction forces (GRF) (1000 Hz); and a 16-channel wireless EMG system (Cometa, Milan, Italy) recorded surface EMG signals from 16 lower limb muscles (1000 Hz) (Sartori et al., 2012a). Participants were barefoot and performed a maximal vertical countermovement jump (Padulo et al., 2013), 10 walking trials over a 10-metre walkway at a self-selected speed (1.17 ± 0.16 m/s), and a series of maximum isometric voluntary contractions (MVC) (Pizzolato et al., 2017) on a dynamometer (Biodex Medical Systems, NY, USA). Hip muscle MVC were acquired with participants standing with the leg in 0° hip abduction, hip flexion, knee flexion, and ankle plantar flexion. Knee and ankle muscle MVC were acquired with participants in a seated position at 80° hip flexion, 30° knee flexion, and 15° ankle plantarflexion.

3. Experimental data processing

Marker trajectories, GRF, and EMG signals were processed using MOtoNMS (Mantoan et al., 2015) in MATLAB (MathWorks, USA). Marker trajectories and GRF were low-pass filtered with a second-order zero-lag Butterworth filter (6 Hz) (Winter et al., 1974). EMG signals were band-pass filtered (30–300 Hz), full-wave rectified, low-pass filtered (6 Hz) (Lloyd and Besier, 2003), and subsequently amplitude-normalised to their maximum values obtained from the dynamic or MVC trials (Lloyd and Besier, 2003). The resulting EMG linear envelopes, now called experimental muscle excitations, were inputs to the EMG-assisted modelling pipeline (Fig. 1) (Pizzolato et al., 2015; Sartori et al., 2014). The hip joint centres were calculated using the Harrington regression equation (Harrington et al., 2007), as recommended by Kainz et al. (2015). The knee and ankle joint centres were calculated as the centre of the medial and lateral markers of the femoral condyles and malleoli, respectively. An offset of 0.27 times the shank length was included for the ankle joint centre (Bruening et al., 2008).

A generic musculoskeletal model (gait2392) was scaled in OpenSim version 3.2 (Delp et al., 2007) to match the anthropometry of each participant (Kainz et al., 2017). The lengths of the femur and tibia were scaled from the joint centres while the torso, pelvis, and foot were scaled using anatomical markers. The 92 muscles were reduced to 34 muscle-tendon units (MTU) actuating one side of the lower limbs (Sartori et al., 2012a). Muscle-tendon operating curves were morphometrically scaled (Modenese et al., 2016), with the final scaled NMS model used in both SO and EMG-assisted modelling pipelines (Fig. 1).

The musculotendon models were different in the EMG-informed and SO methods. The EMG-informed approach used a Hill-type musculotendon model as implemented previously (Buchanan et al., 2004; Lloyd and Besier, 2003). This had muscle force-length-velocity properties and parallel passive muscle force-length relationships that were in series with a compliant tendon. In comparison, we employed OpenSim's standard musculotendon model used in SO, which accounted for the muscle force-length-velocity, but not the passive force contribution, in series with a stiff tendon.

For each walking trial, joint angles, joint moments, MTU lengths and moment arms were calculated using inverse kinematics, inverse dynamics, and muscle analysis tools in OpenSim, respectively. Mean marker RMS errors were 1.41 ± 0.47 cm, while mean RMS residual forces were 3.9 ± 2.2 N and residual moments 26.2 ± 5.1 Nm, so a Reduced Residual Algorithm (Anderson et al., 2006) was not employed to minimise processing time.

Muscle-tendon forces were estimated using either SO in OpenSim, or an EMG-assisted method in the OpenSim plug-in CEINMS (Pizzolato et al., 2015). SO in OpenSim minimised the sum of the muscle activations squared. For the EMG-assisted method, 16 experimental muscle excitations were distributed to the 34 MTU (Sartori et al., 2012a), and its calibration used four walking trials, which was performed in CEINMS. Calibration adjusted the neuromuscular parameters to minimise both peak HJCF and joint moment prediction errors for the hip flexion/extension (FE), hip adduction-abduction (AA), knee flexion/extension (FE), and ankle

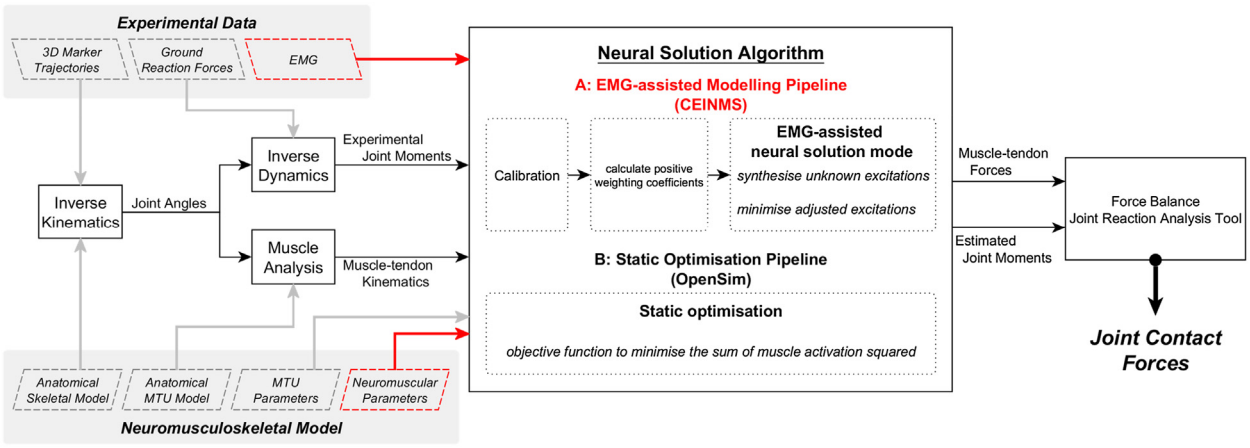

Fig. 1. The overall processing pipeline to estimate joint contact forces. The two pipelines are (A) EMG-assisted modelling pipeline and (B) static optimisation pipeline. The EMG signals and neuromuscular parameters (red) were only used in the EMG-assisted modelling pipeline in CEINMS. The EMG-informed modelling pipeline consisted of calibrating the NMS model, calculating the positive weighting coefficients, and calculating muscle-tendon forces and joint moments using the EMG-assisted neural control solution. The EMG-assisted neural control solution synthesised muscle excitations for the *iliacus* and *psoas major* muscles and minimally adjusted recorded muscle excitations to best balance tracking errors from joint moments and muscle excitations. The static optimisation pipeline utilised static optimisation in OpenSim to calculate muscle-tendon forces and joint moments with an objective function to minimise the sum of the muscle activation squared. (For interpretation of the references to colour in this figure legend, the reader is referred to the web version of this article.)

dorsi/plantar flexion (DPF) joint moments (Sartori et al., 2012a). Minimisation of peak HJCF in the calibration resulted in more physiologically plausible HJCF (Hoang et al., 2018), similar to the results at the knee when minimising KJCF (Gerus et al., 2013). The neuromuscular parameters were tendon slack length, optimal fibre length, maximum isometric force, non-linear shape factor, and EMG-to-activation recursive filter coefficients (Buchanan et al., 2004; Lloyd and Besier, 2003). The calibrated NMS model was used to predict muscle forces using the EMG-assisted method on the remaining six walking trials. In this, the objective function minimised was:

$$f_{obj} = \alpha E_{MOM} + \beta E_{EXC} + \gamma E_{EMG} \quad (1)$$

where E_{MOM} is the sum of the squared differences between estimated and experimental joint moments, E_{EXC} is the sum of squared excitations for all MTUs, E_{EMG} is the sum of the differences between adjusted EMG excitations and recorded EMG excitations, and (α, β, γ) are positive weighting coefficients. The positive weighting coefficients were determined as follows: α was set to 1, and the β and γ weightings (Pizzolato et al., 2015) optimised to concurrently minimise the errors from muscle excitation and joint moment following an established procedure (Sartori et al., 2014). With the estimated muscle-tendon forces from SO and the EMG-assisted neural solutions, HJCF were calculated using the joint reaction analysis tool (Steele et al., 2012) for each approach. The knee and ankle JCF (KJCF and AJCF, respectively) were also calculated.

4. Data analysis

Coefficient of determination (R^2) and root-mean-square error (RMSE) were calculated for the predicted and experimental hip FE, knee FE, and ankle DPF moments (normalised to body mass) for SO and the EMG-assisted methods. In OpenSim, SO matched joint moments by adding reserve actuators, and their contributions were removed to calculate R^2 and RMSE for joint moments to enable comparison with the EMG-assisted neural solutions. R^2 and RMSE were calculated between the predicted and experimental muscle activation patterns for both neural-control solutions. Muscle activations in the EMG-assisted neural solutions were calculated employing the same muscle activation dynamics as per previous studies (Buchanan et al., 2004; Lloyd and Besier, 2003). Muscle co-contraction indices (CCI) for the hip, knee, and ankle flexion-extension moments (M_f and M_e, respectively) were calculated to examine how well EMG-assisted and SO neural solutions predicted muscle co-contraction during stance (Heiden et al., 2009):

$$CCI = \begin{cases} 1 - \frac{M_e}{M_f}, if \ \ M_f > M_e \\ \frac{M_f}{M_e} - 1, otherwise \end{cases} \quad (1)$$

The CCI's reflected the relative muscle co-contraction between flexors and extensors, with 0 = full co-contraction; 1 = no co-contraction and only extensor activation; and −1 = no co-contraction and only flexor activation. Absolute mean CCI's were calculated for four phases of stance: loading (0–15%), early (15–40%), mid (40–60%), and late (60–100%). Joint moment R^2, muscle activation R^2, and mean CCI for each part of stance predicted from the EMG-assisted and SO neural solutions were compared using paired t-tests.

JCF's were normalised to body weight. Resultant JCF peaks for the hip ($HJCF_{peak1}$ and $HJCF_{peak2}$), knee ($KJCF_{peak1}$ and $KJCF_{peak2}$), and ankle ($AJCF_{peak}$) were calculated for the EMG-assisted and SO approaches and compared with available instrumented hip implant data (n = 10, age = 56.9 ± 5.2 yr, body mass = 88.7 ± 12.4 kg, height = 174 ± 5.9 cm, walking speed = 1.1 m/s, 12 months post-operation) and knee implant data (n = 8, age = 72.5 ± 5.0 yr, body mass = 91.4 ± 12.6 kg, height = 172 ± 3.9 cm, walking speed = 1.1 m/s, 12 and 24 months post-operation) (Bergmann et al., 2016, 2014) using a one-way analysis of variance (ANOVA). A Bonferroni correction was applied to account for multiple comparisons. Since instrumented data were unavailable for the ankle, a paired *t*-test was used to compare $AJCF_{peak}$ predicted from the EMG-assisted and SO neural solutions. SPSS Ver. 24 (IBM, USA) with $p < 0.05$ was used for all statistics.

5. Results

The EMG-assisted and SO neural solutions both produced high R^2 (>0.95) and low RMSE (<0.15 Nm/kg) for hip FE, knee FE, and ankle DPF moments compared to experimental data (Fig. 4). R^2 for hip and knee FE were not significantly different between approaches, while R^2 for ankle DPF did differ significantly

($p = 0.001$). The EMG-assisted neural solutions produced lower RMSE than SO for hip FE (0.11Nm/kg vs 0.15Nm/kg) and knee FE moments (0.07Nm/kg vs 0.14Nm/kg), but higher RMSE for the ankle DFPF moments (0.14Nm/kg vs 0.05Nm/kg).

The muscle activations from the EMG-assisted neural solutions produced high R^2 and low RMSE for all muscles when compared to experimental EMG data (Fig. 2). Compared to SO, the EMG-assisted neural solutions also had significantly higher R^2 ($p < 0.001$) with lower RMSE ($p < 0.001$) metrics for all muscles. Compared to experimental EMG data, the EMG-assisted neural solutions produced $R^2 > 0.95$ for all muscles except the adductor group (0.59), while SO solutions had $R^2 > 0.8$ for only two muscles (*lateral hamstring* and *lateral gastrocnemius*) (Fig. 2).

Compared to SO, the EMG-assisted neural solutions generally produced greater co-contraction, i.e. lower CCIs (Fig. 3, Table 1). EMG-assisted neural solutions had significantly lower mean hip FE CCIs during loading ($p < 0.001$), early ($p < 0.001$), mid ($p < 0.001$) and late ($p = 0.03$) stance phases. Knee FE CCIs were also lower in early ($p < 0.001$) and mid ($p = 0.001$) stance, while lower ankle DPF CCIs were observed in loading ($p < 0.001$), early ($p < 0.001$), mid ($p < 0.001$) and late ($p < 0.001$) stance phases.

The estimated JCF peaks from the EMG-assisted neural solutions were significantly higher than those from SO for the hip ($p < 0.001$ for both $HJCF_{peak1}$ and $HJCF_{peak2}$) (Table 2). The $KJCF_{peak1}$ ($p = 0.02$) and $KJCF_{peak2}$ ($p < 0.001$) were significantly higher for EMG-assisted than SO neural solutions, while the $AJCF_{peak}$ estimates did not differ between the EMG-assisted and SO neural solutions.

The EMG-assisted neural solutions estimated significantly higher $HJCF_{peak1}$ ($p = 0.03$) compared to instrumented data, although there were no differences for $HJCF_{peak2}$ ($p = 0.36$) (Table 2). Compared to instrumented data, the SO estimated JCF did not differ significantly for $HJCF_{peak1}$ ($p = 0.08$), yet were significantly lower for $HJCF_{peak2}$ ($p < 0.001$). Although the EMG-assisted and SO neural solutions estimated significantly different KJCF peaks, neither $KJCF_{peak1}$ nor $KJCF_{peak2}$ from either approach were significantly different to the instrumented data.

6. Discussion

This study's objective was to determine if EMG-assisted NMS modelling is appropriate to estimate physiologically plausible HJCF in people with hip OA, in that it well matches the available experimentally measured data (i.e. joint moments and muscle activations) and plausible predictions of *in vivo* HJCF (Bergmann et al., 2016). We also compared two modelling methods to estimate HJCF: (i) SO in OpenSim using a linearly-scaled model with scaled muscular parameters (Modenese et al., 2016); and (ii) the EMG-assisted approach in CEINMS using a linearly-scaled model with calibrated neuromuscular parameters (Pizzolato et al., 2015). Compared to SO, the EMG-assisted method predicted higher HJCF, greater levels of co-contraction, and overall, better tracked experimental data.

Joint moments estimated from the EMG-assisted and SO neural solutions were comparable to the results of inverse dynamics for hip FE, knee FE, and ankle DPF joint moments (Fig. 4). However, SO poorly predicted experimental muscle activations (Fig. 4), perhaps because SO assumes an optimal neuromuscular control strategy, without accounting for the unique activation patterns across individuals (Buchanan and Shreeve, 1996). Nonetheless, SO in OpenSim has been regularly employed to predict JCF in both healthy and pathological populations (Graham et al., 2016; Steele et al., 2012; Wesseling et al., 2016b) due to its simplicity of use. Conversely, muscle activations from the EMG-assisted neural solutions closely resembled experimental muscle activations (Fig. 2), with the exception of the adductor muscle group, albeit still superior to SO estimates. In part, the poorly matched results from the EMG-assisted neural solutions may be due to low-quality surface EMG recordings from the adductors, as a consequence of frequent contact between electrode and contralateral leg.

Lower CCI (i.e. more co-contraction between muscle groups) were observed using the EMG-assisted method compared to SO for hip FE, knee FE, and ankle DPF (Table 1). Notably, these lower CCI were consistently closer to experimental CCI during all four phases of stance (Fig. 3). The directionality of the CCI from SO was also characterised by rapid changes, indicating activation of either agonist or antagonist muscle groups and absence of co-contraction (Fig. 3). This contrasts with both the experimental data and the EMG-assisted neural solutions, which show CCI closer to zero, indicating higher co-contraction during walking.

The EMG-assisted approach predicted higher HJCF than SO (Table 2, Fig. 4). In a previous study, the EMG-assisted neural solutions estimated similar HJCF to the SO neural-control solutions; however, these were in healthy people who exhibited minimal muscle co-contraction (Hoang et al., 2018). Muscle co-contraction affect JCF estimates (Challis, 1997; Gottlieb, 2000;

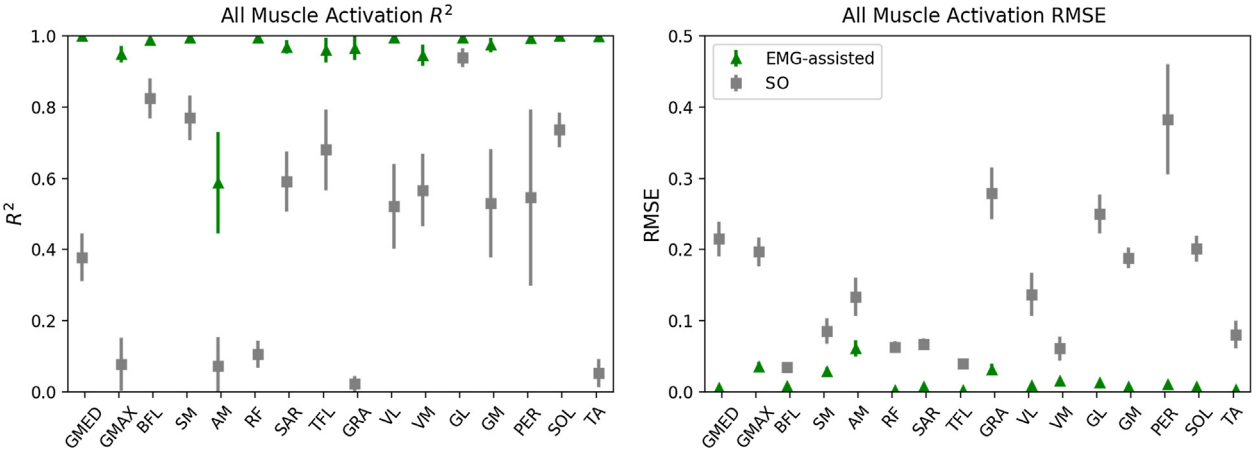

Fig. 2. Muscle activation R^2 and RMSE predicted from the EMG-assisted neural control solution (EMG-assisted) and static optimisation (SO) for all recorded EMGs. Muscles recorded were: *gluteus medius* (GMED), *gluteus maximus* (GMAX), *lateral hamstring group* (HL), *medial hamstring group* (HM), *adductor group* (AG), *rectus femoris* (RF), *sartorius* (SAR), *tensor fascia latae* (TFL), *gracilis* (GRA), *medial vastus lateralis* (VL), *vastus medialis* (VM), *lateral gastrocnemius* (GL), *gastrocnemius* (GM), *peroneus* (PR), *soleus* (SOL), and *tibialis anterior* (TA). The EMG-assisted neural control solution predicted better matching activation for all muscles with lower RMSE than static optimisation. AG was the only muscle with a low R^2 value (<0.6) from the EMG-assisted neural control solution, albeit still higher than that generated from static optimisation.

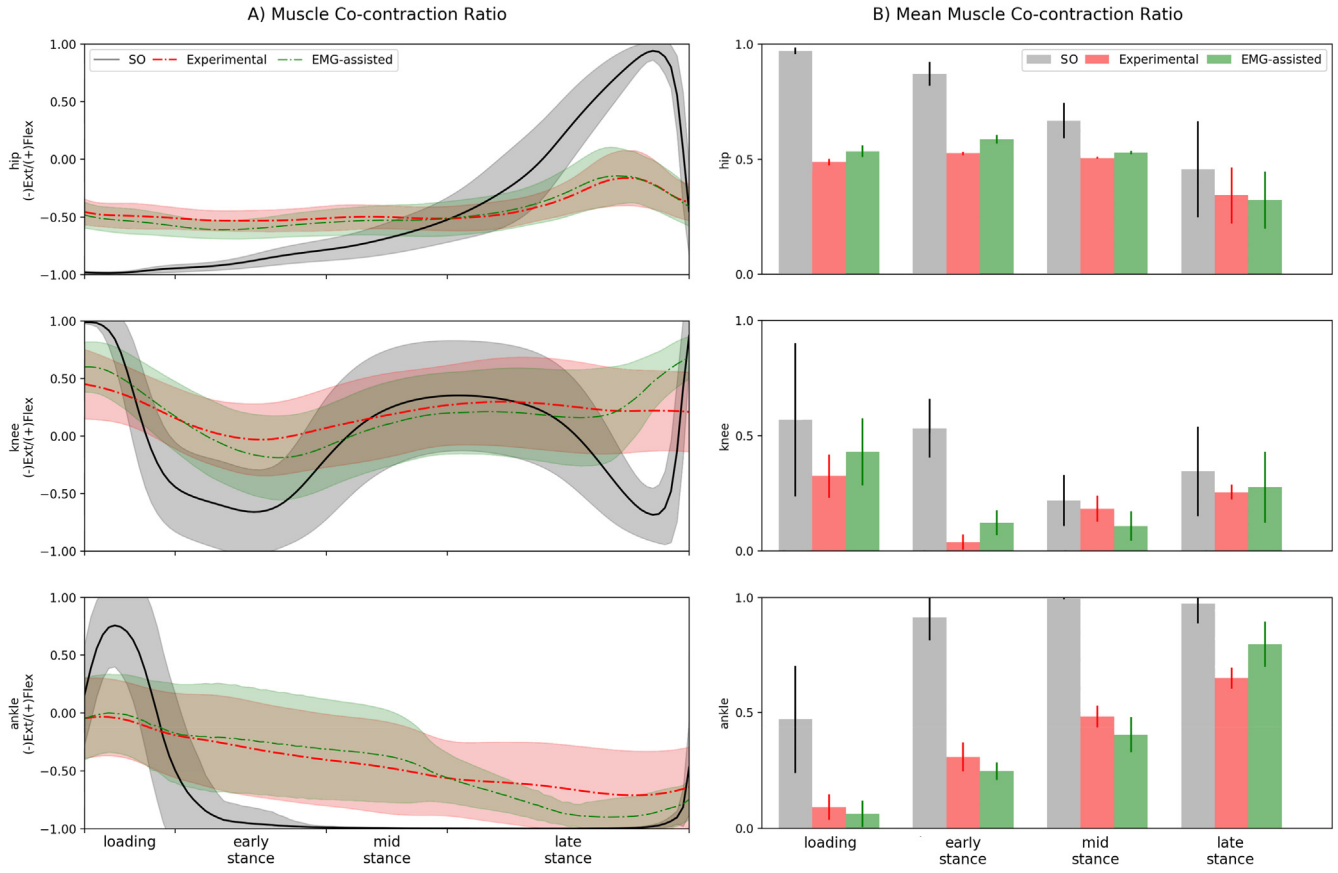

Fig. 3. The muscle co-contraction ratio (CCI) calculated for the EMG-informed neural control solution (EMG-assisted) and static optimisation (SO) are shown with experimental recorded muscle CCI. (A) The muscle CCI during the stance phase (CCI: 0 = full co-contraction; 1 and −1: no co-contraction). (B) The mean muscle CCI during the four phases of stance: loading [0–15%], early [15–40%], mid [40–60%], and late [60–100%] (CCI: 0 = full co-contraction; 1 and −1: no co-contraction).

Table 1
Comparison of co-contraction ratios between the EMG-assisted neural control solution and static optimisation during the four parts of stance phase (loading [0–15%], early [15–40%], mid [40–60%], and late [60–100%]) for each joint.

Joint	Stance phase							
	Loading (0–15%)		Early (15–40%)		Mid (40–60%)		Late (60–100%)	
	p-Value	95% CI of mean difference*	p-value	95% CI of mean difference*	p-value	95% CI of mean difference*	p-value	95% CI of mean difference*
Hip	**<0.001**	−0.4515 to −0.4224	**<0.001**	−0.3123 to −0.2576	**<0.001**	−0.1786 to −0.1014	**0.03**	−0.2529 to −0.01783
knee	0.118	−0.3160 to 0.03815	**<0.001**	−0.4771 to −0.3418	**0.001**	−0.1718 to −0.0481	0.247	−0.1885 to 0.05031
ankle	**<0.001**	−0.5252 to −0.2903	**<0.001**	−0.7188 to −0.6133	**<0.001**	−0.6274 to −0.5524	**<0.001**	−0.2392 to −0.1131

Bold indicates significant at $p < 0.05$.
* Mean difference (EMG-assisted neural control solution – Static optimisation).

Hughes et al., 1995), and differences in HJCF between approaches in this study were the direct result of the EMG-assisted neural solutions correctly accounting for the increased levels of muscle co-contraction (Park et al., 1999; Zeni et al., 2010) evident in our hip OA participants (Table 1, Fig. 3).

When compared to instrumented hip data (Bergmann et al., 2016), the EMG-assisted method predicted higher HJCF, while SO predicted lower HJCF (Table 2, Fig. 4). Although data from instrumented implants are representative of a different patient population (i.e. 12-month post THR vs mild-to-moderate hip OA), they still provide essential insight into which neural-control solution predicts more physiologically plausible HJCF. In previous studies, individuals with THR demonstrated decreased muscle strength compared to healthy controls (Fukumoto et al., 2013; Shih et al., 1994). Although direct comparison of muscle strength between data from Bergmann et al., (2016) and our cohort is not possible, it has been shown that muscle weakness increases with disease progression (Loureiro et al., 2013). This study's cohort are at an earlier stage of hip OA; thus, greater muscle strength is potentially present in our cohort and may, in part, have contributed to the higher HJCF compared to individuals with instrumented implants, since muscle forces are main contributors to HJCF during walking (Correa et al., 2010). Furthermore, the EMG-assisted method also better predicted external joint moments (Fig. 4), muscle activations (Fig. 2), and CCI (Fig. 3) when compared to SO. Collectively, these findings suggest that the EMG-assisted approach predicted more physiologically plausible HJCF than SO.

Contrary to previous NMS modelling studies using SO (Heller et al., 2001; Modenese et al., 2011; Stansfield et al., 2003), $HJCF_{peak2}$ was lower than instrumented hip data. However, these studies employed different SO criteria and/or musculoskeletal models, and compared their HJCF results to a different dataset (Bergmann

Table 2
Hip joint contact force (HJCF), knee joint contact force (KJCF), and ankle joint contact force (AJCF) predicted from the EMG-assisted neural control solution (EMG-assisted) and static optimisation (SO). HJCF and KJCF peaks were compared with instrumented data (Bergmann 2016 and Bergmann 2014, respectively).

Joint contact force		Comparison		p-value
HJCF	peak 1	SO	EMG-assisted	**<0.001** [a]
		SO	Bergmann 2016	0.08 [a]
		EMG-assisted	Bergmann 2016	**0.03** [a]
	peak 2	SO	EMG-assisted	**<0.001** [a]
		SO	Bergmann 2016	**<0.001** [a]
		EMG-assisted	Bergmann 2016	0.15 [a]
KJCF	peak 1	SO	EMG-assisted	**0.02** [a]
		SO	Bergmann 2014	0.19 [a]
		EMG-assisted	Bergmann 2014	0.36 [a]
	peak 2	SO	EMG-assisted	**<0.001** [a]
		SO	Bergmann 2014	0.063 [a]
		EMG-assisted	Bergmann 2014	0.15 [a]
AJCF	peak	SO	EMG-assisted	0.66[b]

[a] One-way ANOVA with Bonferroni adjustment (bold indicates significant at $p < 0.05$).
[b] Paired *t*-test (bold indicates significant at $p < 0.05$).

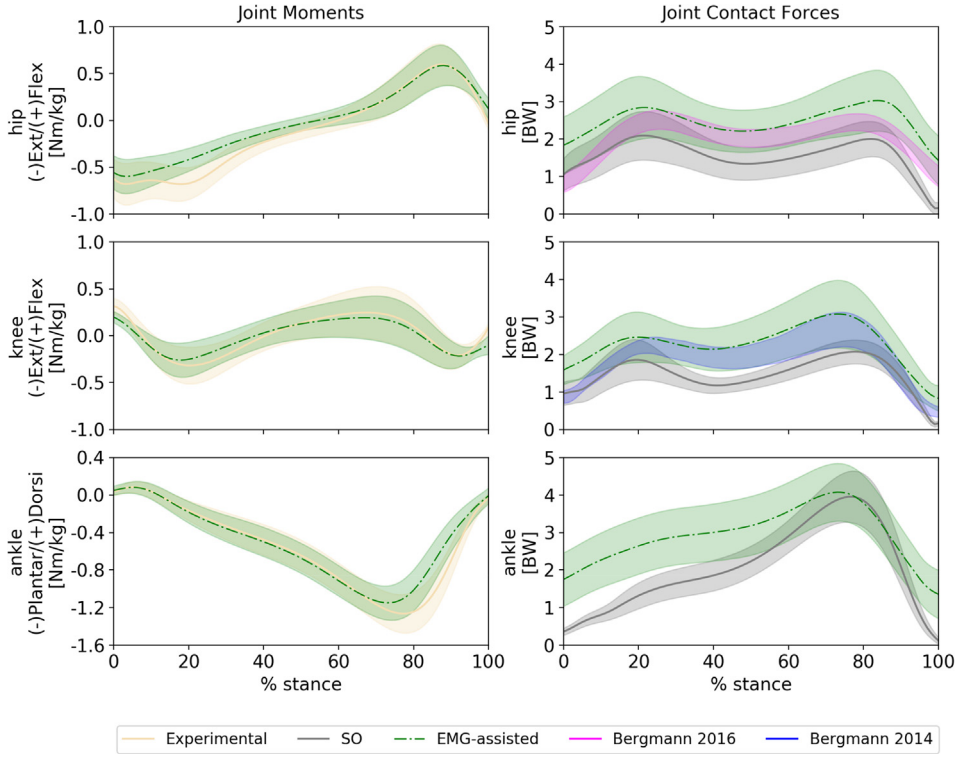

Fig. 4. Joint moment and joint contact forces predicted from the EMG-assisted neural control solution (EMG-assisted) and static optimisation (SO) for the hip, knee, and ankle. Joint moments are shown with experimental joint moments from inverse dynamics (Experimental). Hip joint contact forces (HJCF) are shown with Bergmann et al. (2016) hip data (population: hip OA, n = 10, age = 56.9 ± 5.2 yr, body mass = 88.7 ± 12.4 kg, height = 174 ± 5.9 cm, average walking speed = 1.1 m/s) and knee joint contact forces (KJCF) are shown with Bergmann et al. (2014) instrumented knee data (population: knee OA, n = 8, age = 70.25 ± 5.0 yr, body mass = 91.38 ± 12.6 kg, height = 172.2 ± 3.9 cm, average walking speed = 1.1 m/s). The HJCF and KJCF from Bergmann et al. (2016, 2014) datasets were not from the same subjects; these participant groups differed from our cohort who were in the early stages of hip OA (population: mild-to-moderate hip OA, n = 18, age = 64.0 ± 7.0 yr, body mass = 76.8 ± 14.1 kg, height = 166.0 ± 9.1 cm, average walking speed = 1.17 ± 0.16 m/s).

et al., 2001). Additionally, our process included morphometrically scaled muscle parameters (Modenese et al., 2016), which may explain further discrepancies between our SO results and those of previous studies (Heller et al., 2001; Modenese et al., 2011; Stansfield et al., 2003).

KJCF peaks predicted from the EMG-assisted and SO methods were not significantly different to instrumented knee data (Bergmann et al., 2014). Furthermore, both neural-control solutions predicted similar peak AJCF, although no *in-vivo* data were available for comparison. These comparable knee and ankle JCF further support the premise that greater hip muscle co-contraction underpins the different HJCF estimates, and notably, the more physiologically plausible predictions of the EMG-assisted method.

Some limitations of this study should be considered. Analyses were performed using a linearly-scaled generic musculoskeletal model, which does not account for subject-specific muscle pathways and moment arms, influential factors in estimating JCF's (Lenaerts et al., 2008; Wesseling et al., 2016a). Variation in calculated hip joint centre locations can influence HJCF estimations (Lenaerts et al., 2008; Stagni et al., 2000). However, the same geometries were used for comparing EMG-assisted and SO neural

solutions and thus small errors in hip centre locations are unlikely to change our conclusions. Nevertheless, generic musculoskeletal models remain widely used due to their simplicity and availability (Graham et al., 2016; Kainz et al., 2016; Steele et al., 2012). Future investigation should consider creating musculoskeletal models with subject-specific geometries (Gerus et al., 2013; Wesseling et al., 2016a) and joint kinematics (Brito da Luz et al., 2017).

Calibration of neuromuscular parameters to the individual is necessary (Gerus et al., 2013; Serrancolí et al., 2016) and was performed in the EMG-assisted modelling pipeline. In contrast, calibration was not undertaken in SO (Fig. 1), as generic muscular parameters are routinely used in OpenSim SO studies (Modenese et al., 2011; Steele et al., 2012; Wesseling et al., 2015). Consequently, the muscular parameters (i.e. maximum isometric force, optimal muscle fibre length, tendon slack length) were different between modelling approaches (Figs S1–S3), which would influence the estimation of muscle forces (Garner and Pandy, 2003; Hatze, 1981), the main contributors to JCF (Correa et al., 2010).

Muscle activations were calculated differently between the EMG-assisted method and SO in OpenSim. The EMG-assisted neural solutions estimated muscle activation using a second-order dynamic model (Lloyd and Besier, 2003). Conversely, SO in OpenSim directly calculated muscle activations (Thelen, 2003). Muscle activations estimated by both EMG-assisted and SO approaches were compared to experimental muscle activations, calculated using the same activation model used by the EMG-assisted neural solutions (Lloyd and Besier, 2003). While this may favour EMG-assisted neural solutions over SO, it was the only alternative to compare muscle activations between the two methods. Furthermore, muscle excitations from the *iliacus* and *psoas major* were not recorded due to surface EMG limitations; hence, it was not possible to determine how well the EMG-assisted neural solutions predicted activations from these muscles.

As mentioned previously, the musculotendon models used for the EMG-assisted method and SO in OpenSim were different, i.e. passive force-length contribution with compliant tendon vs no passive force-length contribution with stiff tendon, respectively. Estimation of muscle forces assuming stiff tendons have produced equivocal results; some reporting large errors with large ratios of optimal fibre lengths and tendon slack length (Millard et al., 2013). But the same study also showed little effect at submaximal activation levels, consistent with others who also showed small effects (Sartori et al., 2012b) using stiff tendons in running and sidestepping trials. For the OpenSim models, optimal fibre lengths and tendon slack lengths were initially tuned to ensure muscles operate on the ascending limb and around the peak of the muscle force-length curve (Modenese et al., 2016), reducing the effect of the passive force. In the EMG-assisted method, passive fibre forces were produced but they were low, up to 5% of the optimal fibre force. Nonetheless, the differences between the musculotendon models may have contributed to the differences observed in this study.

Our findings demonstrate that a calibrated EMG-assisted NMS modelling method can predict physiologically plausible HJCF in a population with high levels of co-contraction, including hip OA. Future investigations should consider using the EMG-assisted method to estimate HJCF during more demanding activities (e.g. stair climbing), commonly associated with pain in individuals with hip OA.

Acknowledgements

This work was funded by a Griffith University, Australia postgraduate scholarship (to HXH) and a Griffith University Strategic Investments Grant (to DGL). The authors would like to thank Prof Rod Barrett, A/Prof Monica Reggiani, Dr Peter Mills, Dr Luca Modenese, Dr Aderson Loureiro, Dr Maria Constantinou, Dr Alice Mantoan, Jeremy Higgs, and all participants for their support.

Conflict of interest

The authors declare no conflicts of interest.

Appendix A. Supplementary material

Supplementary data to this article can be found online at https://doi.org/10.1016/j.jbiomech.2018.11.042.

References

Anderson, F.C., John, C.T., Guendelman, E., Arnold, A.S., Delp, S.L., 2006. SimTrack: Software for Rapidly Generating Muscle-Actuated Simulations of Long-Duration Movement. Presented at the 2006 International Symposium on Biomedical Engineering, Taiwan.

Anderson, F.C., Pandy, M.G., 2001. Static and dynamic optimization solutions for gait are practically equivalent. J. Biomech. 34, 153–161. https://doi.org/10.1016/S0021-9290(00)00155-X.

Arnold, A.S., Delp, S.L., 2005. Computer modeling of gait abnormalities in cerebral palsy: application to treatment planning. Theor. Issues Ergon. Sci. 6, 305–312. https://doi.org/10.1080/14639220412331329636.

Bergmann, G., Bender, A., Dymke, J., Duda, G., Damm, P., 2016. Standardized loads acting in hip implants. PLoS One 11, e0155612. https://doi.org/10.1371/journal.pone.0155612.

Bergmann, G., Bender, A., Graichen, F., Dymke, J., Rohlmann, A., Trepczynski, A., Heller, M.O., Kutzner, I., 2014. Standardized Loads Acting in Knee Implants. PLoS One 9, e86035. https://doi.org/10.1371/journal.pone.0086035.

Bergmann, G., Deuretzbacher, G., Heller, M., Graichen, F., Rohlmann, A., Strauss, J., Duda, G.N., 2001. Hip contact forces and gait patterns from routine activities. J. Biomech. 34, 859–871. https://doi.org/10.1016/S0021-9290(01)00040-9.

Brand, R.A., Pedersen, D.R., Davy, D.T., Kotzar, G.M., Heiple, K.G., Goldberg, V.M., 1994. Comparison of hip force calculations and measurements in the same patient. J. Arthroplasty 9, 45–51. https://doi.org/10.1016/0883-5403(94)90136-8.

Brito da Luz, S., Modenese, L., Sancisi, N., Mills, P.M., Kennedy, B., Beck, B.R., Lloyd, D. G., 2017. Feasibility of using MRIs to create subject-specific parallel-mechanism joint models. J. Biomech. 53, 45–55. https://doi.org/10.1016/j.jbiomech.2016.12.018.

Bruening, D.A., Crewe, A.N., Buczek, F.L., 2008. A simple, anatomically based correction to the conventional ankle joint center. Clin. Biomech. 23, 1299–1302. https://doi.org/10.1016/j.clinbiomech.2008.08.005.

Buchanan, T.S., Lloyd, D.G., Manal, K., Besier, T.F., 2004. Neuromusculoskeletal modeling: estimation of muscle forces and joint moments and movements from measurements of neural command. J. Appl. Biomech. 20, 367–395.

Buchanan, T.S., Shreeve, D.A., 1996. An evaluation of optimization techniques for the prediction of muscle activation patterns during isometric tasks. J. Biomech. Eng. – Trans. Asme 118, 565–574. https://doi.org/10.1115/1.2796044.

Challis, J.H., 1997. Producing physiologically realistic individual muscle force estimations by imposing constraints when using optimization techniques. Med. Eng. Phys. 19, 253–261. https://doi.org/10.1016/S1350-4533(96)00062-8.

Correa, T.A., Crossley, K.M., Kim, H.J., Pandy, M.G., 2010. Contributions of individual muscles to hip joint contact force in normal walking. J. Biomech. 43, 1618–1622. https://doi.org/10.1016/j.jbiomech.2010.02.008.

Delp, S.L., Anderson, F.C., Arnold, A.S., Loan, P., Habib, A., John, C.T., Guendelman, E., Thelen, D.G., 2007. OpenSim: open-source software to create and analyze dynamic simulations of movement. IEEE Trans. Biomed. Eng. 54, 1940–1950. https://doi.org/10.1109/TBME.2007.901024.

Farina, D., Negro, F., 2012. Accessing the neural drive to muscle and translation to neurorehabilitation technologies. Biomed. Eng. IEEE Rev. In 5, 3–14. https://doi.org/10.1109/RBME.2012.2183586.

Felson, D.T., 2013. Osteoarthritis as a disease of mechanics. Osteoarthritis Cartilage 21, 10–15. https://doi.org/10.1016/j.joca.2012.09.012.

Fukumoto, Y., Ohata, K., Tsukagoshi, R., Kawanabe, K., Akiyama, H., Mata, T., Kimura, M., Ichihashi, N., 2013. Changes in hip and knee muscle strength in patients following total hip arthroplasty. J. Jpn. Phys. Ther. Assoc. 16, 22–27. https://doi.org/10.1298/jjpta.Vol16_002.

Garner, B.A., Pandy, M.G., 2003. Estimation of musculotendon properties in the human upper limb. Ann. Biomed. Eng. 31, 207–220. https://doi.org/10.1114/1.1540105.

Gerus, P., Sartori, M., Besier, T.F., Fregly, B.J., Delp, S.L., Banks, S.A., Pandy, M.G., D'Lima, D.D., Lloyd, D.G., 2013. Subject-specific knee joint geometry improves predictions of medial tibiofemoral contact forces. J. Biomech. 46, 2778–2786. https://doi.org/10.1016/j.jbiomech.2013.09.005.

Giarmatzis, G., Jonkers, I., Wesseling, M., Van Rossom, S., Verschueren, S., 2015. Loading of hip measured by hip contact forces at different speeds of walking and running. J. Bone Miner. Res. 30, 1431–1440. https://doi.org/10.1002/jbmr.2483.

Gossec, L., Tubach, F., Baron, G., Ravaud, P., Logeart, I., Dougados, M., 2005. Predictive factors of total hip replacement due to primary osteoarthritis: a prospective 2 year study of 505 patients. Ann. Rheum. Dis. 64, 1028–1032. https://doi.org/10.1136/ard.2004.029546.

Gottlieb, G.L., 2000. Minimizing stress is not enough. Motor Control 4, 64–67. discussion 97–116.

Graham, D.F., Carty, C.P., Lloyd, D.G., Lichtwark, G.A., Barrett, R.S., 2014. Muscle contributions to recovery from forward loss of balance by stepping. J. Biomech. 47, 667–674. https://doi.org/10.1016/j.jbiomech.2013.11.047.

Graham, D.F., Modenese, L., Trewartha, G., Carty, C.P., Constantinou, M., Lloyd, D.G., Barrett, R.S., 2016. Hip joint contact loads in older adults during recovery from forward loss of balance by stepping. J. Biomech. 49, 2619–2624. https://doi.org/10.1016/j.jbiomech.2016.05.033.

Harrington, M.E., Zavatsky, A.B., Lawson, S.E.M., Yuan, Z., Theologis, T.N., 2007. Prediction of the hip joint centre in adults, children, and patients with cerebral palsy based on magnetic resonance imaging. J. Biomech. 40, 595–602. https://doi.org/10.1016/j.jbiomech.2006.02.003.

Hatze, H., 1981. Estimation of myodynamic parameter values from observations on isometrically contracting muscle groups. Eur. J. Appl. Physiol. 46, 325–338. https://doi.org/10.1007/BF00422120.

Heiden, T.L., Lloyd, D.G., Ackland, T.R., 2009. Knee extension and flexion weakness in people with knee osteoarthritis: is antagonist cocontraction a factor? J. Orthop. Sports Phys. Ther. 39, 807–815. https://doi.org/10.2519/jospt.2009.3079.

Heller, M.O., Bergmann, G., Deuretzbacher, G., Dürselen, L., Pohl, M., Claes, L., Haas, N.P., Duda, G.N., 2001. Musculo-skeletal loading conditions at the hip during walking and stair climbing. J. Biomech. 34, 883–893.

Hoang, H.X., Pizzolato, C., Diamond, L.E., Lloyd, D.G., 2018. Subject-specific calibration of neuromuscular parameters enables neuromusculoskeletal models to estimate physiologically plausible hip joint contact forces in healthy adults. J. Biomech. 80, 111–120. https://doi.org/10.1016/j.jbiomech.2018.08.023.

Hughes, R.E., Bean, J.C., Chaffin, D.B., 1995. Evaluating the effect of co-contraction in optimization models. J. Biomech. 28, 875–878. https://doi.org/10.1016/0021-9290(95)95277-C.

Kainz, H., Carty, C.P., Modenese, L., Boyd, R.N., Lloyd, D.G., 2015. Estimation of the hip joint centre in human motion analysis: a systematic review. Clin. Biomech. 30, 319–329. https://doi.org/10.1016/j.clinbiomech.2015.02.005.

Kainz, H., Hoang, H., Stockton, C., Boyd, R.R., Lloyd, D.G., Carty, C.P., 2017. Accuracy and reliability of marker based approaches to scale the pelvis, thigh and shank segments in musculoskeletal models. J. Appl. Biomech., 1–21 https://doi.org/10.1123/jab.2016-0282.

Kainz, H., Modenese, L., Lloyd, D.G., Maine, S., Walsh, H.P.J., Carty, C.P., 2016. Joint kinematic calculation based on clinical direct kinematic versus inverse kinematic gait models. J. Biomech. 49, 1658–1669. https://doi.org/10.1016/j.jbiomech.2016.03.052.

Kellgren, J.H., Lawrence, J.S., 1957. Radiological assessment of osteo-arthrosis. Ann. Rheum. Dis. 16, 494–502. https://doi.org/10.1136/ard.16.4.494.

Konrath, J.M., Saxby, D.J., Killen, B.A., Pizzolato, C., Vertullo, C.J., Barrett, R.S., Lloyd, D.G., 2017. Muscle contributions to medial tibiofemoral compartment contact loading following ACL reconstruction using semitendinosus and gracilis tendon grafts. PLoS One 12, e0176016. https://doi.org/10.1371/journal.pone.0176016.

Lenaerts, G., De Groote, F., Demeulenaere, B., Mulier, M., Van der Perre, G., Spaepen, A., Jonkers, I., 2008. Subject-specific hip geometry affects predicted hip joint contact forces during gait. J. Biomech. 41, 1243–1252. https://doi.org/10.1016/j.jbiomech.2008.01.014.

Lloyd, D.G., Besier, T.F., 2003. An EMG-driven musculoskeletal model to estimate muscle forces and knee joint moments in vivo. J. Biomech. 36, 765–776. https://doi.org/10.1016/S0021-9290(03)00010-1.

Lloyd, D.G., Buchanan, T.S., 1996. A model of load sharing between muscles and soft tissues at the human knee during static tasks. J. Biomech. Eng. 118, 367–376.

Loureiro, A., Mills, P.M., Barrett, R.S., 2013. Muscle weakness in hip osteoarthritis: a systematic review. Arthritis Care Res. 65, 340–352. https://doi.org/10.1002/acr.21806.

Mahomed, N.N., Arndt, D.C., McGrory, B.J., Harris, W.H., 2001. The Harris hip score: comparison of patient self-report with surgeon assessment. J. Arthroplasty 16, 575–580. https://doi.org/10.1054/arth.2001.23716.

Manal, K., Buchanan, T.S., 2013. An electromyogram-driven musculoskeletal model of the knee to predict in vivo joint contact forces during normal and novel gait patterns. J. Biomech. Eng. 135, 0210141–0210147. https://doi.org/10.1115/1.4023457.

Mantoan, A., Pizzolato, C., Sartori, M., Sawacha, Z., Cobelli, C., Reggiani, M., 2015. MOtoNMS: A MATLAB toolbox to process motion data for neuromusculoskeletal modeling and simulation. Source Code Biol. Med. 10, 12. https://doi.org/10.1186/s13029-015-0044-4.

Millard, M., Uchida, T., Seth, A., Delp, S.L., 2013. Flexing computational muscle: modeling and simulation of musculotendon dynamics. J. Biomech. Eng. 135, 021005. https://doi.org/10.1115/1.4023390.

Modenese, L., Ceseracciu, E., Reggiani, M., Lloyd, D.G., 2016. Estimation of musculotendon parameters for scaled and subject specific musculoskeletal models using an optimization technique. J. Biomech. 49, 141–148. https://doi.org/10.1016/j.jbiomech.2015.11.006.

Modenese, L., Phillips, A.T., Bull, A.M., 2011. An open source lower limb model: Hip joint validation. J. Biomech. 44, 2185–2193. https://doi.org/10.1016/j.jbiomech.2011.06.019.

Murphy, N.J., Eyles, J.P., Hunter, D.J., 2016. Hip osteoarthritis: etiopathogenesis and implications for management. Adv. Ther. 33, 1921–1946. https://doi.org/10.1007/s12325-016-0409-3.

Padulo, J., Tiloca, A., Powell, D., Granatelli, G., Bianco, A., Paoli, A., 2013. EMG amplitude of the biceps femoris during jumping compared to landing movements. SpringerPlus 2, 520. https://doi.org/10.1186/2193-1801-2-520.

Park, S., Krebs, D.E., Mann, R.W., 1999. Hip muscle co-contraction: evidence from concurrent in vivo pressure measurement and force estimation. Gait Posture 10, 211–222. https://doi.org/10.1016/S0966-6362(99)00033-8.

Pizzolato, C., Lloyd, D.G., Sartori, M., Ceseracciu, E., Besier, T.F., Fregly, B.J., Reggiani, M., 2015. CEINMS: a toolbox to investigate the influence of different neural control solutions on the prediction of muscle excitation and joint moments during dynamic motor tasks. J. Biomech. 48, 3929–3936. https://doi.org/10.1016/j.jbiomech.2015.09.021.

Pizzolato, C., Reggiani, M., Saxby, D.J., Ceseracciu, E., Modenese, L., Lloyd, D.G., 2017. Biofeedback for gait retraining based on real-time estimation of tibiofemoral joint contact forces 1 1 IEEE Trans. Neural Syst. Rehabil. Eng. PP. https://doi.org/10.1109/TNSRE.2017.2683488.

Sartori, M., Farina, D., Lloyd, D.G., 2014. Hybrid neuromusculoskeletal modeling to best track joint moments using a balance between muscle excitations derived from electromyograms and optimization. J. Biomech. 47, 3613–3621. https://doi.org/10.1016/j.jbiomech.2014.10.009.

Sartori, M., Reggiani, M., Farina, D., Lloyd, D.G., 2012a. EMG-driven forward-dynamic estimation of muscle force and joint moment about multiple degrees of freedom in the human lower extremity. PLoS One 7, e52618. https://doi.org/10.1371/journal.pone.0052618.

Sartori, M., Reggiani, M., Pagello, E., Lloyd, D.G., 2012b. Modeling the human knee for assistive technologies. IEEE Trans. Biomed. Eng. 59, 2642–2649. https://doi.org/10.1109/TBME.2012.2208746.

Saxby, D.J., Bryant, A.L., Modenese, L., Gerus, P., Killen, B.A., Konrath, J., Fortin, K., Wrigley, T.V., Bennell, K.L., Cicuttini, F.M., Vertullo, C., Feller, J.A., Whitehead, T., Gallie, P., Lloyd, D.G., 2016a. Tibiofemoral contact forces in the anterior cruciate ligament-reconstructed knee. Med. Sci. Sports Exerc. 48, 2195–2206. https://doi.org/10.1249/MSS.0000000000001021.

Saxby, D.J., Modenese, L., Bryant, A.L., Gerus, P., Killen, B., Fortin, K., Wrigley, T.V., Bennell, K.L., Cicuttini, F.M., Lloyd, D.G., 2016b. Tibiofemoral contact forces during walking, running and sidestepping. Gait Posture 49, 78–85. https://doi.org/10.1016/j.gaitpost.2016.06.014.

Serrancolí, G., Kinney, A.L., Fregly, B.J., Font-Llagunes, J.M., 2016. Neuromusculoskeletal model calibration significantly affects predicted knee contact forces for walking 081001 081001 J. Biomech. Eng. 138. https://doi.org/10.1115/1.4033673.

Shih, C.-H., Du, Y.-K., Lin, Y.-H., Wu, C.-C., 1994. Muscular recovery around the hip joint after total hip arthroplasty. Clin. Orthop. 302, 115–120.

Skalshøi, O., Iversen, C.H., Nielsen, D.B., Jacobsen, J., Mechlenurg, I., Søballe, K., Sørensen, H., 2015. Walking patterns and hip contact forces in patients with hip dysplasia. Gait Posture. https://doi.org/10.1016/j.gaitpost.2015.08.008.

Stagni, R., Leardini, A., Cappozzo, A., Grazia Benedetti, M., Cappello, A., 2000. Effects of hip joint centre mislocation on gait analysis results. J. Biomech. 33, 1479–1487. https://doi.org/10.1016/S0021-9290(00)00093-2.

Stansfield, B.W., Nicol, A.C., Paul, J.P., Kelly, I.G., Graichen, F., Bergmann, G., 2003. Direct comparison of calculated hip joint contact forces with those measured using instrumented implants. An evaluation of a three-dimensional mathematical model of the lower limb. J. Biomech. 36, 929–936. https://doi.org/10.1016/S0021-9290(03)00072-1.

Steele, K.M., DeMers, M.S., Schwartz, M.H., Delp, S.L., 2012. Compressive tibiofemoral force during crouch gait. Gait Posture 35, 556–560. https://doi.org/10.1016/j.gaitpost.2011.11.023.

Thelen, D.G., 2003. Adjustment of muscle mechanics model parameters to simulate dynamic contractions in older adults. J. Biomech. Eng. 125, 70–77.

Thelen, D.G., Schultz, A.B., Fassois, S.D., Ashton-Miller, J.A., 1994. Identification of dynamic myoelectric signal-to-force models during isometric lumbar muscle contractions. J. Biomech. 27, 907–919. https://doi.org/10.1016/0021-9290(94)90263-1.

van den Bogert, A.J., Read, L., Nigg, B.M., 1999. An analysis of hip joint loading during walking, running, and skiing. Med. Sci. Sports Exerc. 31, 131–142.

Wang, M., Shen, J., Jin, H., Im, H.J., Sandy, J., Chen, D., 2011. Recent progress in understanding molecular mechanisms of cartilage degeneration during osteoarthritis. Ann. N. Acad. Sci. 1240, 61–69. https://doi.org/10.1111/j.1749-6632.2011.06258.x.

Wellsandt, E., Gardinier, E.S., Manal, K., Axe, M.J., Buchanan, T.S., Snyder-Mackler, L., 2016. Decreased knee joint loading associated with early knee osteoarthritis after anterior cruciate ligament injury. Am. J. Sports Med. 44, 143–151. https://doi.org/10.1177/0363546515608475.

Wesseling, M., Derikx, L.C., de Groote, F., Bartels, W., Meyer, C., Verdonschot, N., Jonkers, I., 2015. Muscle optimization techniques impact the magnitude of calculated hip joint contact forces. J. Orthop. Res. 33, 430–438. https://doi.org/10.1002/jor.22769.

Wesseling, M., Groote, F.D., Bosmans, L., Bartels, W., Meyer, C., Desloovere, K., Jonkers, I., 2016a. Subject-specific geometrical detail rather than cost function formulation affects hip loading calculation. Comput. Methods Biomech. Biomed. Eng., 1–14 https://doi.org/10.1080/10255842.2016.1154547.

Wesseling, M., Groote, F.D., Meyer, C., Corten, K., Simon, J.-P., Desloovere, K., Jonkers, I., 2016b. Subject-specific musculoskeletal modelling in patients before and

after total hip arthroplasty. Comput. Methods Biomech. Biomed. Eng., 1–9 https://doi.org/10.1080/10255842.2016.1181174.
Winter, D.A., Sidwall, H.G., Hobson, D.A., 1974. Measurement and reduction of noise in kinematics of locomotion. J. Biomech. 7, 157–159. https://doi.org/10.1016/0021-9290(74)90056-6.
Zeni, J.A., Rudolph, K., Higginson, J.S., 2010. Alterations in quadriceps and hamstrings coordination in persons with medial compartment knee osteoarthritis. J. Electromyogr. Kinesiol. 20, 148–154. https://doi.org/10.1016/j.jelekin.2008.12.003.